J. Micromech. Microeng. **13** (2003) 548–556 PII: S0960-1317(03)55237-8

Thermal and mechanical analysis of micromachined gas sensors

J Puigcorbé[1], D Vogel[2], B Michel[2], A Vilà[1], I Gràcia[3], C Cané[3] and J R Morante[3]

[1] Electronic Materials and Engineering (EME), Department of Electronics, Marti i Franques 1, 08028 Barcelona, Catalunya, Spain
[2] Fraunhofer Institute Reliability and Microintegration (IZM), Berlin, Germany
[3] Centre Nacional de Microelectrònica, Bellaterra, Barcelona, Spain

E-mail: jpuigcor@el.ub.es

Received 24 October 2002, in final form 2 April 2003
Published 14 May 2003
Online at stacks.iop.org/JMM/13/548

Abstract
In this paper, we present a complete thermomechanical study of a micromachined gas sensor substrate. The work has been carried out combining coupled electrothermomechanical three-dimensional finite element modelling simulations with electrical, infrared thermography and interferometric microscopy experimental measurements. The performances predicted by simulations, such as the power consumption (heating efficiency in air of 5.7 °C mW^{-1}), the time response (19 ms), the membrane deflection during operation and the preferential failure sites in the micromachined substrate have been confirmed by experience. Their good agreement validates the model, and allows us to consider the adaptability of this design as a micromachined substrate for integrated gas sensors.

1. Introduction

Recent trends on metal–oxide gas sensors require low power consumption, fast response, uniform temperature distribution over the sensing material and good mechanical stability at high temperatures. These demanding requirements, together with the thermal isolation from the surrounding elements, can be best achieved by mounting the metal oxide on a thermal isolated structure, generally a dielectric membrane, obtained by means of silicon micromachining technology [1].

In this type of microsensor, the active area comprises a heater, sensor electrodes and the gas-sensitive layer placed at the centre of a thin membrane, which provides thermal isolation between the heated active area and the outer frame [2–4]. The correct operation of the gas sensor needs good temperature uniformity over the whole gas-sensitive layer and very low thermal inertia allowing for the response of the device to be fast enough [5]. This is especially important when working in temperature-pulsed operation mode, as suggested by various authors [6, 7] in order to reduce the power consumption and to enhance the selectivity.

This working principle implies a rapid and frequent change in temperature which, as well as the temperature gradients over the active area, causes important thermal stresses that can shorten the lifetime of the sensor. Although a major issue of free-standing dielectric oxide/nitride membranes is their mechanical stability, it is well known that CMOS thin films exhibit residual mechanical stress strongly dependent on the process sequence and on the deposition technique used. In micromachined membranes, this residual stress is compressive and induces an undesired bending of the structure after the fabrication process. However, the major contribution of mechanical stress is the thermal stress induced during the operation of the integrated micro-heater. The high temperature achieved during operation can even produce cracks or delamination of the films that compose the stacked structure.

In this paper, we present a thermomechanical study of a micromechanized gas sensor. Our objective is to investigate its thermal and mechanical behaviour for a typical operation temperature between 20–650 °C combining experimental electrical, infrared and interferometric microscopy measurements and electrothermomechanical simulations. Special attention has been focused on the thermal distribution, the thermal stresses induced in the membrane and the structure deflection at different operational temperatures.

0960-1317/03/050548+09$30.00 © 2003 IOP Publishing Ltd Printed in the UK

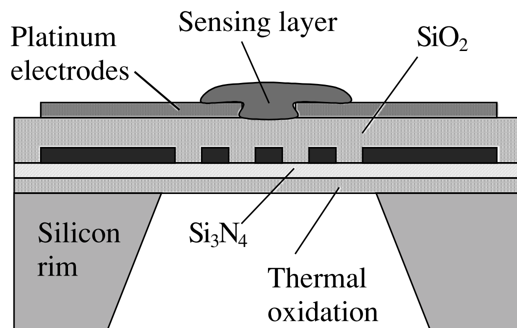

Figure 1. Cross-section sketch of the stacked membrane.

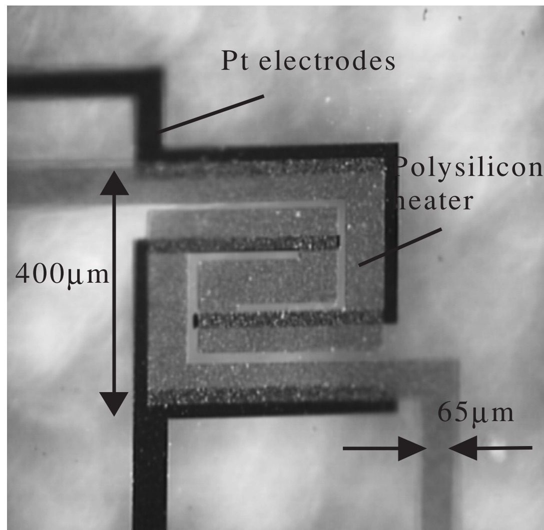

Figure 2. Membrane configuration considered and electrode geometry.

2. Description of the sensor structure

The device is schematically depicted in figure 1. The micromachined substrates were fabricated on double side polished p-type ⟨100⟩ Si substrates, 300 μm thick. A layer of 0.3 μm of LPCVD Si_3N_4 has been used as a dielectric membrane. The spiral-shaped micro-heater is doped polysilicon (640 Ω) and a layer of deposited SiO_2, 0.8 μm thick, acts as electrical isolation to the top. Locally, Pt electrodes (0.3 μm thick), which provide electrical contact with the sensing layer, patterned with lift-off, are included. This stacked films configuration provides an active area of $400 \times 400\ \mu m^2$ at the centre of a membrane of 1×1 mm^2. The lines configuring the micro-heater were 65 μm wide elsewhere and spaced by 15 μm. Finally, silicon bulk micromachining from the back side was carried out with KOH. The micromachined gas sensor is shown in figure 2.

3. Finite element model and material properties

The commercial finite element model (FEM) program ANSYS [8] has been employed for the coupled electrothermal and mechanical simulations by means of a three-dimensional (3D) model. Heat conduction through the membrane and conduction to the air were considered as the two dominant heat-transfer factors. Additionally, for temperatures higher than 400 °C, the radiation losses have also been considered. The boundary conditions for the thermal analysis assume that room temperature is preserved at the external part of the silicon chip. The thermal equilibrium on the membrane has been considered as the result of heat exchange between the heat generated in the electrical resistance through the Joule effect and the heat loss mechanisms of convection and conduction towards the cooler supporting massive material. Consequently, on the upper and lower surfaces of the membrane, the heat is dissipated through convective and conductive exchange with air. Due to the small size of the heated structures, the convection losses are negligible at median-low temperatures [9]. Assuming the fluid motion to be negligible, the air has been considered as a static fluid modelled as a solid on the top and bottom of the membrane. The extension of the air that has to be modelled can be found first by simulating only a small volume of air around the structure, and then by increasing the distance in successive simulations until the convergence of the heat exchange. In our test structures, distances higher than 0.5 mm produce negligible ($<$1%) changes in the total heat transfer. Experimental evidence for the applicability of this assumption has been found in the literature [9, 10].

For temperatures higher than 400 °C, the heat losses due to radiation have been included in the simulations considering the active area as a grey emitter with an emissivity of 0.6 obtained from infrared thermography measurements and in agreement with [11]. The methodology to determine this value will be explained in more detail in the electrothermal analysis (section 4).

The thermal conductivity of the thin films can differ significantly from the bulk value for the same material and depends on the fabrication conditions, processes and thickness. The difference between the thermal conductivities of thin films and the corresponding bulk material implies that the thermal conductivity of the analysed membrane is *a priori unknown*. Preliminary electrothermal FEM simulations and electrical and thermography measurements have been combined in order to obtain the thermal conductivities of the layers. The power consumption of different test micro-hotplates has been fitted by numerical simulations in order to determine the thermal conductivity of the membrane materials. Figure 3 shows one of the tested micro-hotplates and its temperature distribution obtained by simulation. Figure 4 compares the experimental and simulated power consumption of the tested devices. The initial thermal conductivities employed in this characterization process have been obtained from the extended work carried out by Arx [12], which reports on the thermal properties of CMOS thin films such as chemical vapour deposition (CVD) oxides, nitrides and polycrystalline silicon. The material properties used for the simulations and those obtained from the data in the literature are listed in table 1 [12–18].

The temperature distribution obtained in the electrothermal simulations constitutes the load for the thermomechanical simulations. Linear elastic behaviour has been assumed for all materials. Finally, due to the large deflections induced in the membrane, the simulations include non-linear large geometric effects.

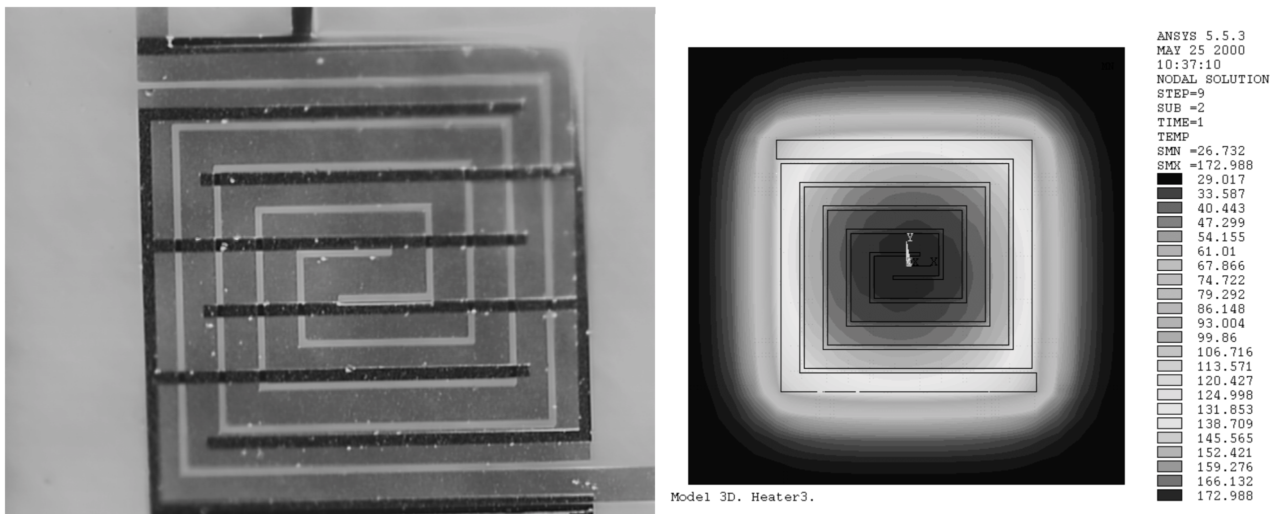

Figure 3. Thermal test micro-hotplate and its temperature distribution.

Table 1. Thermal conductivity, coefficient of thermal expansion and Young's Modulus for the considered materials.

Material	Thermal conductivity K (W (mK)$^{-1}$) Calculated	Literature	Coefficient of thermal expansion α (10^{-6} °C^{-1})	Young's modulus (GPa)
Silicon nitride	22	22.7 [13]	2.4 [16]	370 [17]
Silicon oxide	1.5	1–1.6 [13–15]	0.6 [16]	70 [17]
PolySilicon	20	18–29 [12, 14]	2.8 [16]	160 [18]

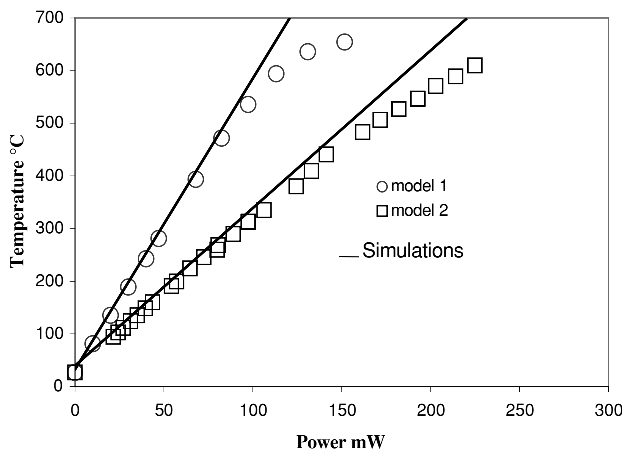

Figure 4. Measured and simulated power consumption of test micro-hotplates. Model 1 refers to the investigated design shown in figure 2. Model 2 refers to the test design shown in figure 3.

4. Electrothermal analysis

A uniform micro-heater temperature is a necessary requirement as it allows the correct operation of the gas sensor. The temperature uniformity depends on the membrane materials and also on their geometry, especially that of the micro-heater.

Electrothermal simulations reveal that the maximum current density obtained is around 6×10^8 A m^{-2} when 10 V is applied to the micro-heater, inducing an average temperature in the active area of 600 °C, see figure 5. For higher current densities (>$1 - 10 \times 10^9$ A m^{-2}) electromigration effects have been reported with accompanying resistance changes attributed to redistribution of dopant species [19]. These problems can be discarded in gas sensor applications usually working up to 450 °C.

The temperature gradient in the active area generated by this current density is approximately 0.3 °C μm^{-1}, as shown in figure 6. Experimental infrared thremography measurements have confirmed the validity of our FEM, as shown in figure 7.

The infrared camera Thermovision® 900 System from AGEMA Infrared Systems AB (pixel size 22 μm) was used in order to acquire the temperature distribution in the membrane. The apparent emissivity of the membrane surface was fixed to 0.7 for lower temperatures (up to 300 °C) and 0.5 at higher temperatures. These values were determined by comparing the average temperature in the micro-heater obtained from thermography (micro-heater pixel integration) and from electrical (I–V) measurements. A comparison between infrared thermography and electrical measurements is shown in figure 8.

The power consumption of the micro-hotplate obtained from FEM simulations has been compared with experimental results, in which the polysilicon heater, previously calibrated, has been used as a thermometer. These electrical measurements reveal that an input power of 65 mW applied to the heater produces an operating temperature in the active area of around 400 °C (heating efficiency of 5.7 °C mW^{-1}), see figure 9. Up to 350 °C, the experimental results and the linear simulations agree quite well. Above this temperature, it is necessary to take into account the temperature dependence of the thermal conductivity of the surrounding air ($K_{\mathrm{air}} = f(T°)$) and the radiation losses. This new procedure provides better agreement with experimental

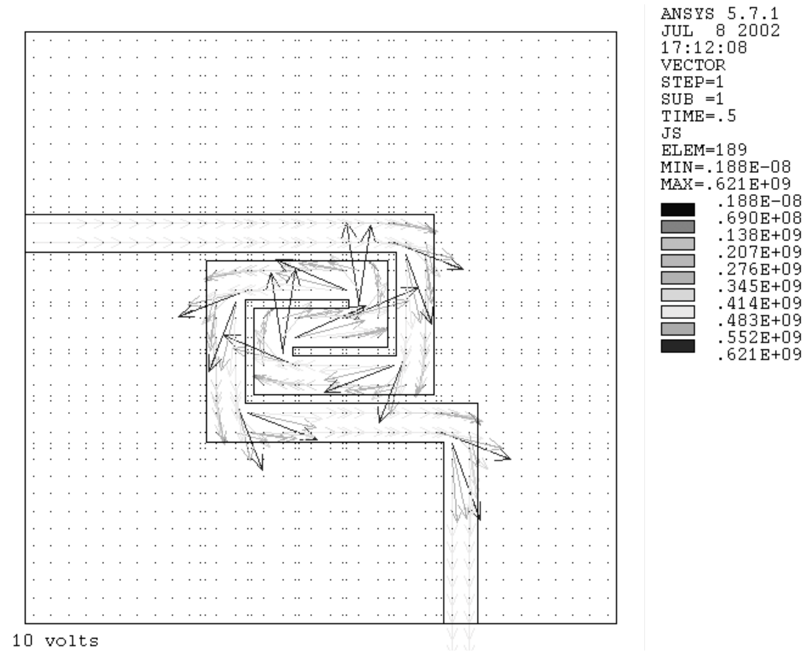

Figure 5. Simulated current density in the micro-heater for an input voltage of 10 V.

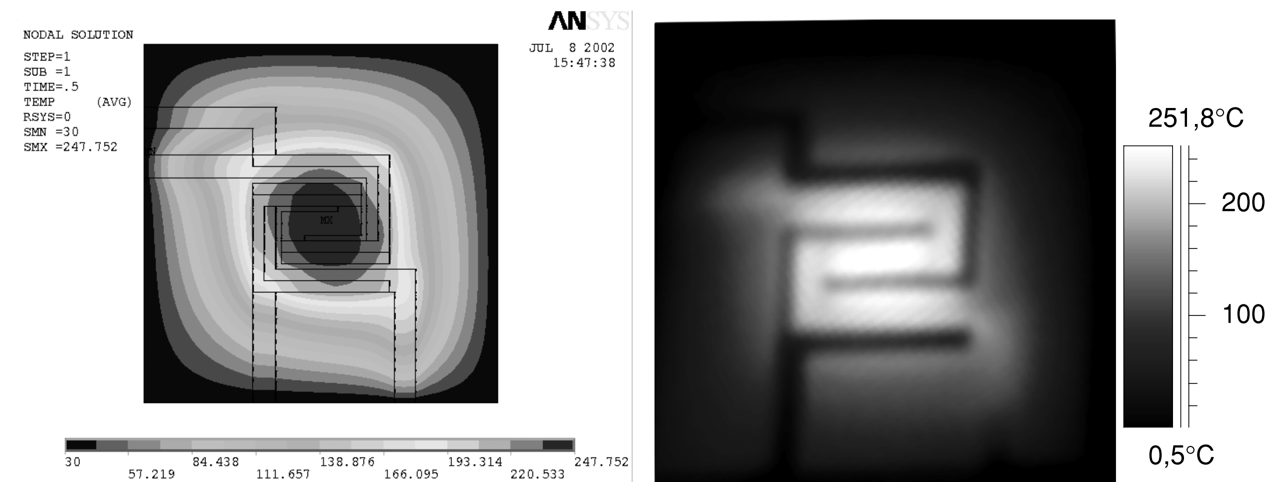

Figure 6. Simulated and infrared thermography temperature distribution over the membrane for an input power of 30 mW (5 V).

results than linear simulations, as shown in figure 9. However, at high temperatures, there remains a slight difference (around 5–10%) which can be related with fluid motion losses [9].

On the other hand, the transient response of the structure was determined by placing the device within a Wheatstone bridge. After this, a square wave with a dc offset was applied. The equilibrium temperature (see figure 10) was reached within 19 ms, which corresponds to the rise time measured from 10 to 90%. The obtained transient response is two orders of magnitude lower than the time response of the sensing layer and agrees very well with the FEM dynamic simulations, as is also shown in figure 10.

5. Thermomechanical behaviour

The difference between the thermal expansion coefficients in the stacked membrane (see table 1), together with the temperature gradients and in time–temperature variations, produces thermal-induced strain and stress that causes undesirable structure deflections.

The thermal-induced stress simulations were also performed in ANSYS using the previous temperature distribution as a load for the mechanical model. In order to ensure the convergence and to avoid numerical instabilities related with the membrane buckling and following the strategy of Ziebart *et al* [20], the simulations were undertaken by the application of the previous thermal loads together with an out-of-plane temporary pressure. Moreover, first the membrane was loaded with a differential pressure, then the thermal load was applied together with the pressure, and finally the pressure was removed releasing the structure to the thermal-induced position.

No material non-linearity has been taken into account because silicon oxide, silicon nitride and polysilicon have

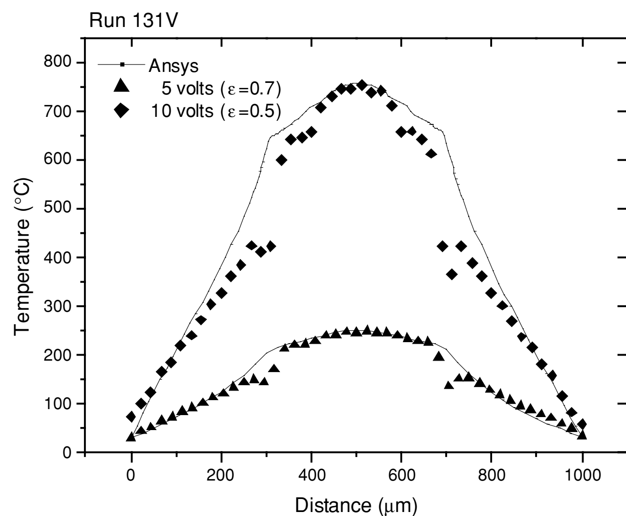

Figure 7. Experimental and simulated temperature profile along the membrane for an input power of 30 mW (5 V) and 97 mW (10 V).

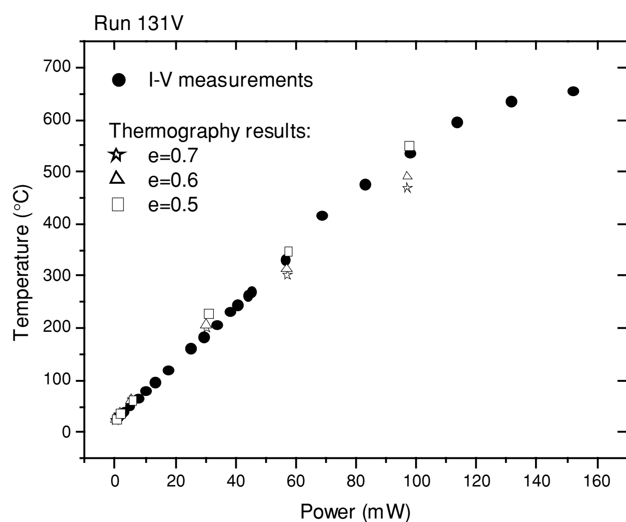

Figure 8. Relation between average heater temperature and power in the micro-heater obtained from infrared thermography and electrical (*I*–*V*) measurements. The thermography measurements consider different emissivities.

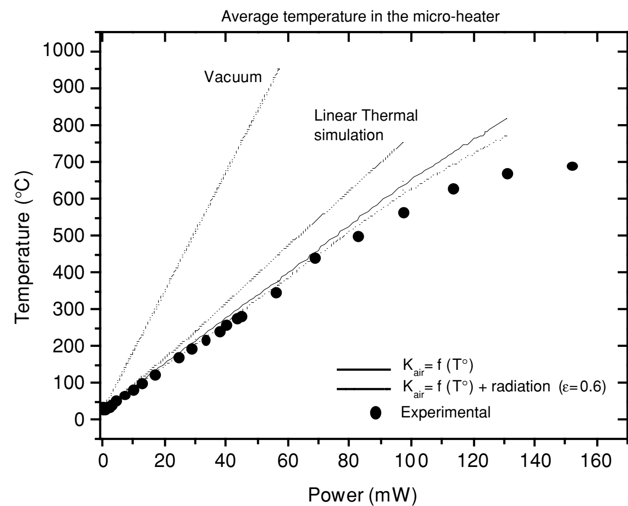

Figure 9. Relation between average heater temperature and power consumption in the micro-heater: measured (points) and simulated (line). There is, only at high temperatures, a slight discrepancy between simulated and experimental results.

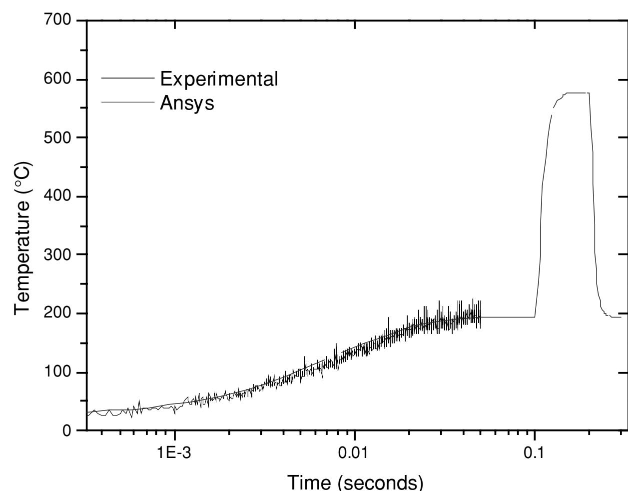

Figure 10. Measured and simulated thermal dynamic behaviour of the sensor substrate for an input voltage of 5 V. Notice that the temperature reached is the average temperature all along the micro-heater.

linear elastic behaviour until fracture. Moreover, the large-deflection behaviour has been analysed by means of geometric non-linear simulations.

5.1. Residual stress in the membrane

From the mechanical point of view, the first objective was to evaluate the residual stresses that operate in the membrane after the fabrication process. The membrane deflection measurement has been carried out using interferometric surface analysis microscopy (Zygo) equipment. The measured membrane deflection value combined with the large-deflection theory of uniformly loaded diaphragms permits us to calculate the average stress in the membrane. The approximate load–deflection relation for membranes has been extensively treated in [21].

At room temperature, the residual bending of the analysed membranes is around 7 μm. Figure 11 shows the topography map of the residual deflection of the membrane obtained by interferometric measurements. The average residual stress required to produce this deflection is –20 MPa. This resultant stress is within the acceptable range of $|\sigma_{\text{residual}}| < 0.1$ GPa which avoids the membrane breakage [11]. Above this stress range, the membrane is jeopardized, and problems such as film delamination or the structure crack cannot be discarded.

The situation may change at the different working temperatures of the micro-heater.

5.2. Membrane deflection during operation

Heating of the sensor produces the thermal expansion of the stacked layers introducing additional stresses that affect the membrane deflection. For our studied membrane configuration, when heating, it is expected that the mechanical

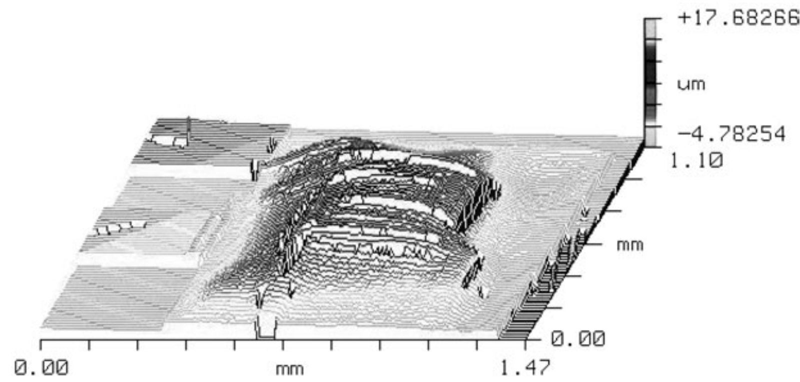

Figure 11. Measured residual vertical deflection of the membrane at room temperature after the fabrication process.

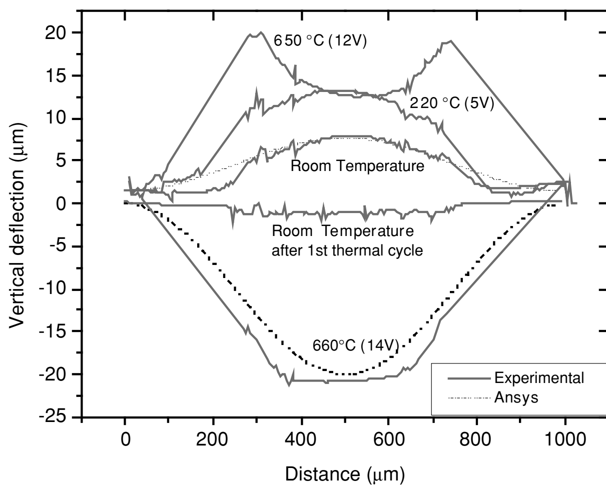

Figure 12. Experimental and simulated vertical deflection of the membrane, at different operating voltages. It is remarcable that after the first heating cycle the initial deflection at room temperature has reduced considerably.

stability will be guaranteed because the critical stress, i.e. the axial equivalent stress that causes the buckling of the membrane, is around –5 MPa. This stress is lower by far than the initial residual stress (−20 MPa), thus the membrane deflection is in post-buckling behaviour.

Due to the layer configuration of the stacked membrane, when heating, the bimetallic effect [21, 22] causes the structure to bend downwards. However, the upward residual deflection of the membrane increases when medium voltages are applied, as shown in figure 12. In this situation, the bending moment caused by the membrane expansion, which increases the amount of bowing, is larger than the moment produced by the bimetallic effect [23].

Further increasing the input power, and thus the temperature, only the centre part of the membrane area bends downwards, inverting the initial direction as shown in figure 12. The interferometric microscopy measurement of this behaviour is shown in figure 13. The change of the bending direction is related with the fact that the active area, i.e. the area covered by the micro-heater, is hotter than the rest of the membrane, as has been reported in the thermal analysis. This temperature difference induces the expansion of the active area from the membrane, and thus it bends relatively to the remainder material. This bimetallic effect dominates in the active area at moderate-high temperatures (above 450 °C),

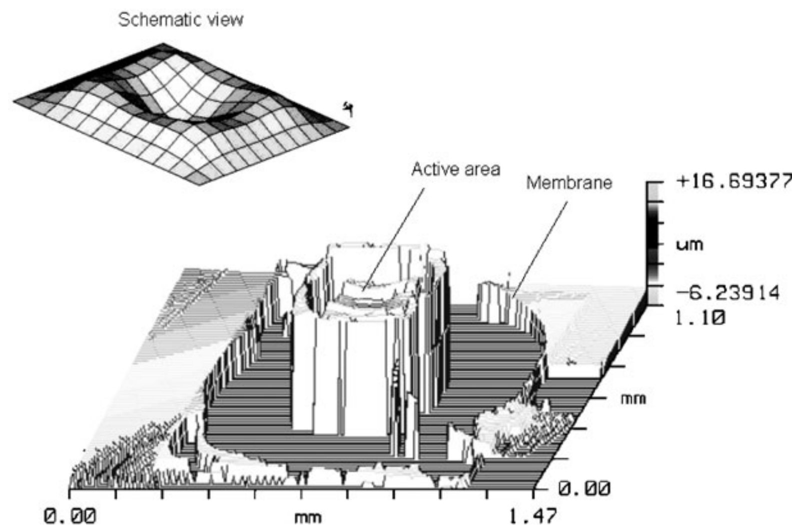

Figure 13. Measured deflection map of the membrane at 575 °C, in the first heating cycle. The inversion of the bending is clearly visible in the central part of the membrane, in which is located the micro-heater.

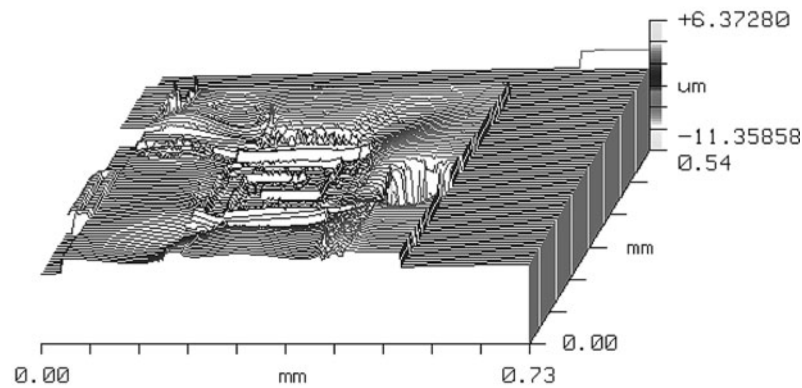

Figure 14. Measured deflection map of the membrane at room temperature after the first heating cycle. The residual bending is reduced considerebly up to -1 μm.

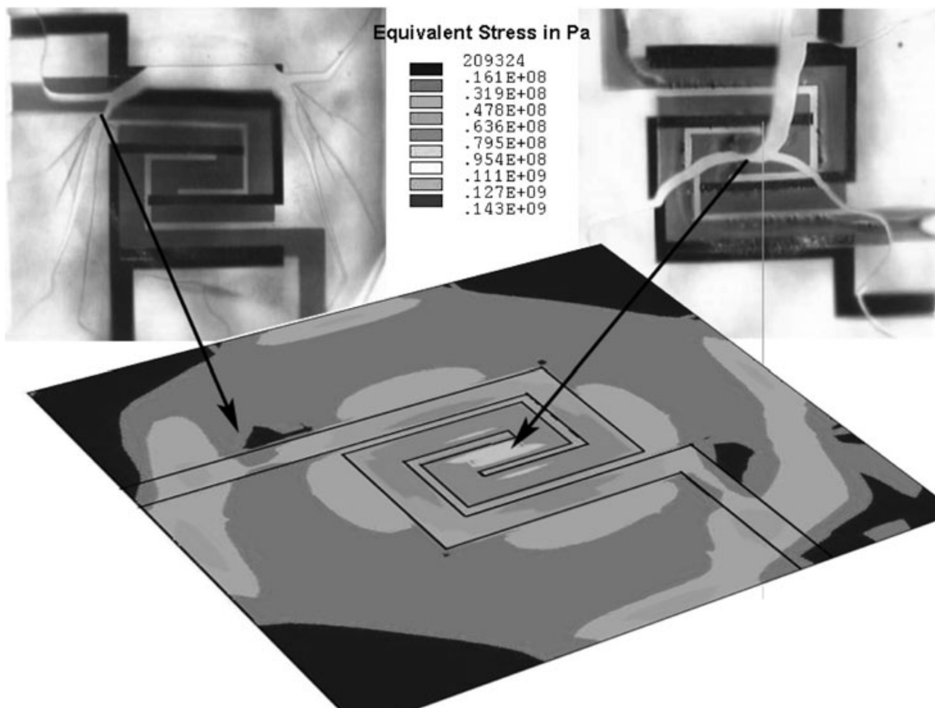

Figure 15. Broken membrane after increasing the temperature above 650 °C, and equivalent stresses obtained from FEM model. The highest stress areas agree very well with the rupture zones.

inverting the initial upward deflection. In this situation, there coexist in the membrane an upward deflection due to the thermal expansion against the fixed walls and a bimetallic downward deflection at the membrane centre. Both effects coexist up to around 575 °C (12 V) in the active area. From this point, slight system perturbation produces the sudden total inversion of the membrane downwards, as shown in figure 12.

After this, the membrane deflects always downwards due to the bimetallic effect caused by the stacked configuration of the membrane. The maximum measured deflection before the rupture is -21 μm, which corresponds to an average temperature in the active area around 650 °C. For higher temperatures in the membrane, the thermal-induced stresses produce fracture in its central part and the structure cracks.

After a first heating cycle up to 575 °C in the active area, new profile measurement shows that the residual deflection has been reduced to –1 μm approximately, as shown in figure 14. The partial reduction of the residual stress is related to temperature relaxation mechanisms and grain growth of thin films during high temperature operation. Therefore, further mechanical simulations have been carried out taking into account no initial bending. The good agreement between predicted and experimental deflections shown in figure 12 validates the mechanical model.

5.3. Cracking by thermal-induced stress

The experimental analysis reveals that for temperatures between 20–650 °C the membrane stability is guaranteed. The situation changes for temperatures higher than 650 °C. In this case, the excessive bending of the structure together with the high-induced stresses cause the crack of the membrane. Before the rupture, the maximum measured deflection is -21 μm. The average stress required to produce this deflection

is around −150 MPa, which is in agreement with the rupture values reported by Rossi *et al* [11].

Figure 15 shows the stress developed in the membrane when the device is heated from 20 to 650 °C. The distribution obtained from the thermo-mechanical simulations predicts different stress areas. The first one is located close to the membrane edges, along a median line of the membrane, and a second one, just on the membrane centre. Also, it appears a ring-shaped zone, around the active area. Among these zones, the most important one is located at the centre of the micro-heater, where the stress distribution follows the direction of the micro-heater line. The stress variation obtained from simulations agrees very well with the initial fracture zone in the cracked membrane. From ours FEM simulations, at 650 °C, the maximum change of stress is around −210 MPa (compressive) in silicon nitride, 170 MPa in silicon oxide and −180 MPa in the polysilicon micro-heater. These stresses, induced during the operation of the sensor, reduce the intrinsic residual stress of silicon nitride (tensile residual stress) and silicon oxide (compressive) [11].

During the high temperature operation of the sensor, AFM measurements have revealed the formation of hillocks and voids in the SiO_2 film induced by the grain growth process. These results suggest that voids in SiO_2, which is the less stiff material in the membrane [17], combined with the change of stress from the residual compressive to tensile state can produce the crack formation.

6. Conclusions

A laboratory optimized micro-hotplate has been developed and tested in order to characterize its thermal and mechanical behaviour by combining experimental measurements with FEM simulations.

The performances predicted by the numerical model, such as the power consumption, the time response, the vertical deflection and the membrane rupture are in good accordance with experimental electrical, infrared thermography and interferometric measurements.

Electrothermal investigations reveal that the tested sensor substrate provides low thermal inertia (<19 ms) and heating efficiencies in air of 5.7 °C mW^{-1}, with good temperature distribution in the active area (temperature gradient 0.3 °C μm^{-1}). For temperatures higher than 350 °C we have included in our simulations the temperature dependence of the thermal conductivity of the surrounding air and the radiation losses. This new procedure has provided better agreement with experimental results than linear simulations.

From the thermomechanical point of view, the experimental analysis shows that for temperatures between 20–650 °C the membrane stability is guaranteed. A first heating cycle is enough for relaxing the initial stress produced as a result of the thermal treatments during the fabrication process. The measurement of the membrane deflection at different operating temperatures has validated the mechanical simulations, and thus allows us to obtain the thermal-induced stresses in the dielectric layers using the same models. In this context, the maximum equivalent stress has been identified at the centre and along the edge of the active area of the micro-hotplate. This suggests that these zones are preferential failure sites in the structure. For temperatures above 650 °C, the induced stress is large enough to produce the structure crack, as confirmed by the experimental and the simulated analyses.

The investigation methodology and the obtained results have provided criteria and design rules for the analysis and optimization of micromachined gas sensors.

Acknowledgment

The Eureka-Eurimus Program MICROBOILER EM47 predominantly finances the main work presented in this paper.

References

[1] Göpel W and Schierbaum K D 1995 SnO_2 sensors: current status and future trends *Sensors Actuators* B **26–27** 1–2
[2] Dibbern U 1990 A substrate for thin film gas sensors in microelectronic technology *Sensors Actuators* B **2** 63–70
[3] Briand D, Krauss A, van der Schoot B, Weimar U, Barsan N, Göpel W and de Rooij N F 2000 Design and fabrication of high-temperature micro-hotplates for drop-coated gas sensors *Sensors Actuators* B **68** 223–33
[4] Astié S, Gué A M, Scheid E and Guillemet J P 2000 Design of a low power SnO_2 gas sensor integrated on silicon oxynitride membrane *Sensors Actuators* B **67** 84–8
[5] Götz A, Gràcia I, Cané C and Lora-Tamayo E 1997 Thermal and mechanical aspects for designing micromachined low power gas sensors *J. Micromech. Microeng.* **7** 247–9
[6] Heiling A, Barsan N, Weimar U, Schweizer-Berverich M, Gardner J W and Göpel W 1997 Gas identification by modulating temperatures of SnO_2-based thick film sensors *Sensors Actuators* B **43** 45–51
[7] Cavicchi R E, Suehle J S, Kreider K G, Gaitan M and Chaparal P 1996 Optimized temperature-pulse sequences for the enhancement of chemically specific response patterns from micro-hotplate gas sensors *Sensors Actuators* B **33** 142–6
[8] ANSYS Reference Manual Swanson Analysis Systems Inc. Houston, PA.
[9] Götz A 1997 Integrated microsensors for microsystems with application in biomedicine and environmental control *PhD Thesis* Universitat Autònoma de Barcelona, Spain
[10] Lang W 1990 Heat transport from a chip *IEEE Trans. Electron Devices* **17** 4
[11] Rossi C, Temple-Boyer P and Estève D 1998 Realization and performance of thin $SiO_2/SiNx$ membrane for microheater applications *Sensors Actuators* A **64** 241–5
[12] Arx M 1998 Thermal properties of CMOS thin films *PhD Thesis* ETH Zurich
[13] Rossi C, Scheid E and Esteve D 1997 Theoretical and experimental study of silicon micromachined microheater with dielectric stacked membranes *Sensors Actuators* A **3** 183–9
[14] Paul O and Baltes H 1993 Thermal conductivity of CMOS materials for the optimization of microsensors *J. Micromech. Microeng.* **3** 110–2
[15] Gallard S, Tallarida G, Borghesi A and Zanotti L 1999 Thermal conductivity of SiO_2 films by scanning thermal microscopy *J. Non-Cryst. Solids* **245** 203–9
[16] Shinha A K, Levinstein H J and Smith T E 1978 Thermal stresses and cracking resistance of dielectric films (SiN, Si_3N_4 and SiO_2) on Si substrates *J. Appl. Phys.* **49** 4
[17] Yoshioka T, Ando T, Shikida M and Sato K 2000 Tensile testing of SiO_2 and Si_3N_4 films carried out on a silicon chip *Sensors Actuators* **82** 291–6
[18] Maier-Schneider D, Köprülülü A, Ballhausen S and Obermeier E 1996 Elastic properties and microstructure of LPCVD polysilicon films *J. Micromech. Microeng.* **6** 436–46

[19] Parameswaran M, Robinson A M, Blackburn D L, Gaitan M and Geist J 1991 Micromachined thermal radiation emitter from a commercial CMOS process *IEEE Electron Device Lett.* **12** 57–9

[20] Ziebart V, Paul O and Baltes H 1999 Strongly buckled square micromachined membranes *J. Microelectromech. Syst.* **8** 4

[21] Timoshenko S and Woinowsky-Krieger S 1987 *Theory of Plates and Shells* (New York: McGraw-Hill)

[22] Suhir E 1989 Interfacial stresses in bimetallic thermostats *J. Appl. Mech.* **56** 595–600

[23] Puers R, Cozma A and Bruyker D D 1998 On the mechanisms in thermally actuated composite diaphragms *Sensors Actuators* A **67** 13–17